Nucleic Acids Research, 2024, **52**, 5596–5609
https://doi.org/10.1093/nar/gkae198
Advance access publication date: 23 March 2024
Gene regulation, Chromatin and Epigenetics

The zinc-finger protein Z4 cooperates with condensin II to regulate somatic chromosome pairing and 3D chromatin organization

Marta Puerto[1,2,†], Mamta Shukla[3,†], Paula Bujosa[1,2], Juan Pérez-Roldán[1,2], Mònica Torràs-Llort[1,2], Srividya Tamirisa[1,2], Albert Carbonell[1,2], Carme Solé[2,4], Joynob Akter Puspo[3], Christopher T. Cummings[5], Eulàlia de Nadal[2,4], Francesc Posas[2,4], Fernando Azorín[1,2,*] and M. Jordan Rowley[3,*]

[1]Institute of Molecular Biology of Barcelona, IBMB, CSIC, Baldiri Reixac 4, 08028 Barcelona, Spain
[2]Institute for Research in Biomedicine of Barcelona, IRB Barcelona. The Barcelona Institute of Science and Technology. Baldiri Reixac 10, 08028 Barcelona, Spain
[3]Department of Genetics, Cell Biology and Anatomy, University of Nebraska Medical Center, Omaha, NE, USA
[4]Department of Medicine and Life Sciences (MELIS), Universitat Pompeu Fabra (UPF), Barcelona, Spain
[5]Department of Pediatrics, University of Nebraska Medical Center, Omaha, NE, USA

[*]To whom correspondence should be addressed. Email: fambmc@ibmb.csic.es
Correspondence may also be addressed to M. Jordan Rowley. Tel: +1 402 836 9794; Fax: +1 402 559 9020; Email: jordan.rowley@unmc.edu
[†]The first two authors should be regarded as Joint First Authors.

Abstract

Chromosome pairing constitutes an important level of genome organization, yet the mechanisms that regulate pairing in somatic cells and the impact on 3D chromatin organization are still poorly understood. Here, we address these questions in *Drosophila*, an organism with robust somatic pairing. In *Drosophila*, pairing preferentially occurs at *loci* consisting of numerous architectural protein binding sites (APBSs), suggesting a role of architectural proteins (APs) in pairing regulation. Amongst these, the anti-pairing function of the condensin II subunit CAP-H2 is well established. However, the factors that regulate CAP-H2 localization and action at APBSs remain largely unknown. Here, we identify two factors that control CAP-H2 occupancy at APBSs and, therefore, regulate pairing. We show that Z4, interacts with CAP-H2 and is required for its localization at APBSs. We also show that hyperosmotic cellular stress induces fast and reversible unpairing in a Z4/CAP-H2 dependent manner. Moreover, by combining the opposite effects of Z4 depletion and osmostress, we show that pairing correlates with the strength of intrachromosomal 3D interactions, such as active (A) compartment interactions, intragenic gene-loops, and polycomb (Pc)-mediated chromatin loops. Altogether, our results reveal new players in CAP-H2-mediated pairing regulation and the intimate interplay between inter-chromosomal and intra-chromosomal 3D interactions.

Graphical abstract

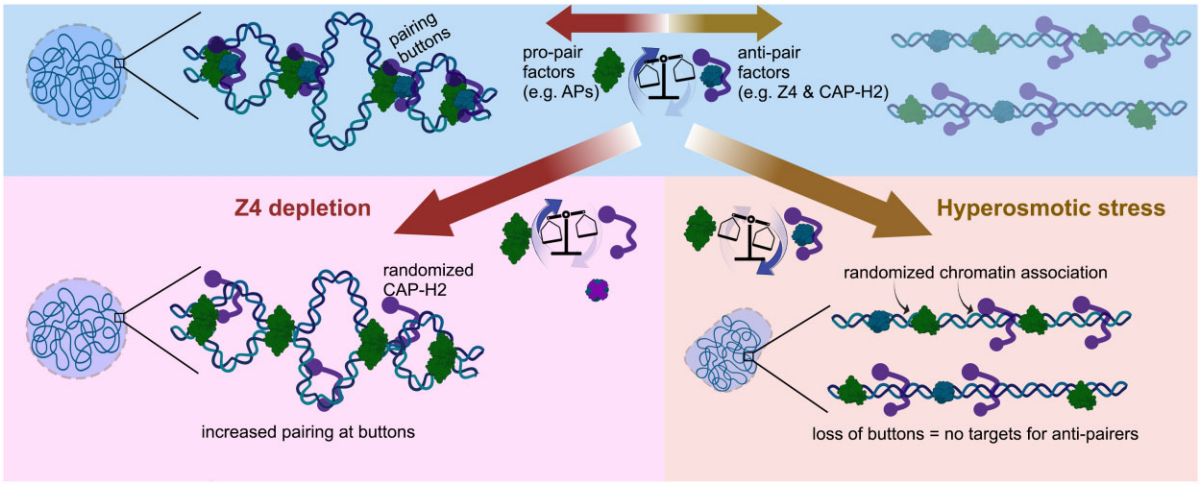

Received: October 24, 2023. **Revised:** February 16, 2024. **Editorial Decision:** March 4, 2024. **Accepted:** March 7, 2024

Introduction

Eukaryotic chromatin is arranged within a 3D nuclear context, the architecture of which is intimately associated with transcriptional regulation. Several hallmarks of chromatin organization have been described, from chromosome territories and compartments to topologically associating domains (TADs) and chromatin loops (for a recent review, see (1)). Chromosome pairing represents an additional level of genome organization. For example, sister chromatids remain tightly paired along their length after DNA replication (reviewed in (2–4)). In addition, homologous chromosomes extensively pair in germ cells during meiosis and, to a lesser extent, in somatic cells (reviewed in (5–7)). An extensive somatic pairing of homologues was first reported in Diptera (8). In particular, *Drosophila* homologues form end-to-end pairing interactions throughout interphase (7,9,10). These interactions are important for gene regulation, and the pairing of homologues has been found in somatic cells throughout most stages of development (7,11–20). Outside of *Drosophila*, the extent of somatic pairing of homologues is still a matter of debate. However, in response to specific cellular processes and/or developmental cues, localized pairing interactions between homologues have been identified in multiple species, including mammals (5–7). In humans, extensive homolog pairing appears to be associated with disease (6,7).

Increasing evidence suggests that, in *Drosophila* interphase somatic cells, pairing interactions are not uniformly distributed along the chromosome, and it has been proposed that sites of high pairing are located frequently across the genome, acting as 'buttons' to promote the close association of paired chromosomes (11–14,17). In general, pairing buttons overlap genomic *loci* consisting of numerous architectural protein binding sites (APBSs), and it is thought that combinations of architectural proteins (APs) cooperate to modulate pairing (11,15,19). It is currently unclear if the buttons for sister pairing and homologue pairing represent the same *loci*. Additionally, while buttons represent sites of 'tight' pairing, recent haplotype-resolved Hi-C analyses showed the presence of 'loose' pairing interactions that involve non-identical fragments in a 'register shifted' manner (12,14).

Chromosome pairing represents a balance between antipairers and factors that promote pairing. Methods that measure general pairing, such as FISH, have been used to identify proteins that influence pairing. For example, an RNAi screen in *Drosophila* identified multiple genes that have pairing-promoting and anti-pairing activity (21). Many of these pairing factors are well evolutionarily conserved (22). Among these is CAP-H2, a subunit of the condensin II complex that binds to APBSs *loci* (7,9–11,23–25) and has a well-known function as an anti-pairer (7,11,26). However, little is known about the factors that regulate CAP-H2 localization and function at APBSs, or the actual contribution of the rest of APs to pairing interactions. Here, to analyze chromosome pairing, we have used a recently developed Hi-C approach that infers chromosomal pairing interactions from the orientation of ligation between identical sequence fragments (11). This approach creates 1D signal tracks that detail the intensity of Hi-C derived pairing (hd-pairing) across the genome, resulting in the identification of tightly paired *loci* at high genomic resolution. Using this approach, we show here that the zinc-finger protein Z4/putzig, which is another AP, interacts with CAP-H2, and is required for CAP-H2 localization and anti-pairing function at APBSs *loci*. In addition, we also show that hyperosmotic stress induces fast/reversible chromosome unpairing that depends on Z4/CAP-H2. It was previously shown that osmostress reduces nuclear volume, promotes chromatin condensation, delocalizes APs into insulator bodies and induces fast/reversible changes to 3D chromatin organization (31–34), but how this impacts chromosome pairing was not known.

How inter-chromosomal pairing interactions impact the other features of 3D chromatin organization is not well understood. It is particularly unclear how *Drosophila* chromosomes can engage in pervasive chromosome pairing throughout interphase while simultaneously maintaining other distinct features of 3D chromatin organization. Despite the extensive and tight pairing of alleles, *Drosophila* Hi-C maps display remarkably similar organizational features to mammals, including strong compartmentalization segregating active (A) from inactive (B) *loci* (11,27). However, unlike mammals, *Drosophila* chromatin does not arrange itself into CTCF loops, and we have shown that *Drosophila* TADs best represent close-range compartmental interactions, forming compartment domains (27). In fact, in *Drosophila*, CTCF is one amongst several other APs that co-occupy APBSs *loci* (11,12,15). *Drosophila* chromatin organization also includes gene loops and Polycomb (Pc) loops (11,26,28–30). Gene-loops are characterized by intra-genic interactions, the intensity of which correlates with transcription elongation (11). Pc-loops are characterized by high-intensity point-to-point interactions anchored by Pc (26,29,30). Here, by combining the opposite effects of osmostress and Z4 depletion on pairing, we illustrate the correlation between inter-chromosomal pairing interactions and intra-chromosomal features of 3D chromatin organization. Our results show that conditions that abolish chromosome pairing, such as osmostress, strongly diminish AA compartment interactions and intragenic gene-loops, while, *vice versa*, increased pairing observed upon Z4 depletion correlates with increased gene-loop and AA interactions. We also show that chromosome pairing reinforces Pc-loop interactions.

Materials and methods

Antibodies

αCap-H2, αZ4 and αDDP1 are described in (35–37) and (38), respectively. The rest of antibodies used were commercially available: αRNAPII (Biolegend, Cat# 664906; RRID:AB_2565554), αTubulin (Millipore, Cat# MAB3408, RRID:AB_94650), αH3 (Cell Signaling, Cat# 9715; RRID:AB_331563), and αPc (Santa Cruz Biotech, Sc-25762), αBEAF-32 (DSHB), αH3S10P (Millipore 06-570) and αLaminB (DSHB ADL67.10).

Cell culture, RNAi and hyperosmotic stress

Drosophila Kc167 cells were cultured in isotonic SFX media. For RNAi knockdown experiments, cells were treated with dsRNAs against Z4 and, as control, against LacZ, using the primers described in Supplementary Table S1. For Z4 knockdown two different dsRNAs were used in combination: dsRNAVDRC and dsRNAPG obtained using the primers from the Vienna *Drosophila* Resource Center Repository and from Silva-Sousa *et al*. (39), respectively. Briefly, at day 0, cells were diluted to 10^6 cells/ml and the dsRNAs added to the media, 20 μg dsRNALacZ/10^6 cells for the LacZ controls and

10 μg dsRNAPG + 10 μg dsRNAVDRC/10^6 cells for the Z4 knock-downs. Cells were incubated for 3 days and, at day 3, diluted again to 10^6 cells/ml and treated with a second dose of dsRNAs as for day 0 for 3 more days. To induce hyperosmotic stress, cells were treated with 300 mM NaCl for 1 h, which is in the range previously used for hyperosmotic stress in *Drosophila* (250–400 mM) (31,32). Recovery conditions included incubation in the above hypertonic media for 1 h followed by incubation in isotonic SFX media for 1 h. Cell viability and p38 phosphorylation status were checked after salt treatment and upon recovery.

Fluorescence microscopy

For Fluorescence *in situ* hybridization (FISH), cells were adhered onto lysine coated slides for 1 h followed by brief washes in PBS for 5 min. Cells were fixed in 4% paraformaldehyde in PBS and washed in 2× SSCT for 5 min at room temperature (RT). Slides were then washed with 2xSSCT/50% formamide for 5 min at RT followed by pre-denaturation in 2xSSCT/50% formamide at 92°C for 2 min and 60°C for 20 min. Hybridization with DNA probes was carried out at 92°C for 3 min by placing DNA probe solution directly onto slides. Slides were then placed in a humidified chamber overnight at RT and mounted with vectashield-DAPI after two washes in 2× SSCT at RT. Cells were imaged with Zeiss LSM 780 confocal microscope. Probes used were: Cy5-359 (Cy5-GGGATCGTTAGCACTGGTAATTAG CTGC) and AACAC-Cy3 (Cy3-AACACAACACAACACAAC ACAACACAACACAACAC) from Integrated DNA Technologies (IDT). For each probe, we considered that the corresponding *loci* were paired in cells showing a single fluorescence signal or several signals separated by <1 μm (21).

When the effect of hyperosmotic stress on nuclear size was determined, cells in isotonic media or after hyperosmotic stress were briefly washed with PBS, fixed in 4% paraformaldehyde and stained with DAPI for 15 min. Then, cells were plated on glass slides and subjected to imaging using SPE confocal microscope. To determine the effect of Z4 depletion on nuclear size, control LacZ and Z4-depleted cells were plated in well plates containing cover slips coated with Concanavalin A (0.5mg/ml; Sigma) and, after 24 h, cells were processed for immunostaining with mouse monoclonal αLaminB (DSHB ADL67.10) (1:2000). For visualization, cover slips were mounted on slides with Mowiol (Calbiochem-Novabiochem) containing 0.2ng/ml DAPI (Sigma) and analyzed in a Leica TCS/SPE confocal microscope equipped with LAS/AF software. Images were acquired and processed using ImageJ (http://imagej.nih.gov/ij/). Volume measurements were performed running the 3D-object counter ImageJ tool. When the effect of Z4 depletion on the morphology of mitotic chromosome was determined, chromosome spreads were performed as described in (40). Briefly, S2 cells were incubated in hypotonic buffer for 5 min, immobilized onto slides by centrifugation for 10 min at 500 rpm with low acceleration in a TermoShandon Cytospin using a single-chamber Cytofunnel and, then, fixed in 4% paraformaldehyde for 10 min. After fixation cells were washed with PBS and permeabilized in 0.5% Triton X-100 in PBS. For visualization, slides were mounted in Mowiol (Calbiochem-Novabiochem) containing 0.2 ng/ml DAPI (Sigma) and analyzed in a Zeiss 880 confocal microscope equipped with Airyscan for image acquisition. Airyscan raw data were preprocessed with the automatic setting of Zen Black and analyzed on ImageJ for chromatid length and thickness measurements.

Co-immunoprecipitation experiments

Co-immunoprecipitation experiments were performed with total extracts. Briefly, 60 ml of confluent Kc167 cells were harvested by centrifugation and the pellet was washed three times with PBS. The washed pellet was dissolved in 1 ml of IP Buffer (50mM Tris–HCl pH 8, 200 mM NaCl, 5 mM EDTA, 0.5% NP-40, Protease Inhibitors cocktail), incubated in ice for 30 min, lysed with a Dounce homogenizer B (35–40 strokes), centrifuged at 3700 g for 15 min at 4°C, and the supernatant was aliquoted and stored at –80°C. For immunoprecipitation, 6 μl of rabbit αCAP-H2 and 2 μl of rabbit αDDP1 (as control) were added to the extracts and incubated on a wheel overnight at 4°C. Then, 30 μl of Protein A sepharose beads (GE Healthcare Life Sciences) were added and incubated for 2 h at 4°C. Beads where recovered by centrifugation and washed 3 times with 1 ml of IP buffer. For elution, beads were resuspended in 2× PLB, β-mercaptoethanol, boiled and spun down, and the supernatants were analyzed by Western Blot (WB).

Western blot (WB) analyses

WB analyses were performed on total extracts, to validate knockdown efficiency, or on crosslinked chromatin prepared exactly as for ChIP-seq in order to directly determine chromatin bound levels. When total cells extracts were analyzed, cells were directly resuspended in PLB (25mM Tris–HCl pH 6.8, 4.35% glycerol, 1% SDS) and boiled before electrophoresis. When crosslinked chromatin was analyzed, cells were fixed with 1.8% formaldehyde and crosslinked chromatin was purified and sonicated as for ChIP according to (41). Note that this step appears to be particularly important for CAP-H2 detection, as previous efforts to detect CAP-H2 in total extracts required GFP tagging/overexpression (35,42). For quantification, autoradiographic films were digitalized using a GS-800 Calibrated Laser Densitometer (Bio-Rad) and quantified using ImageJ Gel Analyzer plugin. Signal from each lane was normalized to the corresponding loading control.

ChIP-seq and ChIP-qPCR

For ChIP-seq, crosslinked chromatin and immunoprecipitation experiments were performed as described previously (41), except that antibody-bound protein complexes were isolated with protein A sepharose beads (GE Healthcare Life Sciences) washed with RIPA buffer (140 mM NaCl, 10 mM Tris–HCl pH 8.0, 1 mM EDTA, 1% Triton X-100, 0.1% SDS, 0.1% DOC) and shortly blocked with RIPA, 1% BSA. The following antibodies were used for immunoprecipitation: guinea pig αZ4 (2 μl), rabbit αCAP-H2 (6 μl) and mouse αRNAPII (4 μl). For sequencing, single-indexed and dual-indexed DNA libraries were generated using the NEBNextUltra II DNA Library Prep kit from Illumina (New England Biolabs). Single-indexed libraries were sequenced 50 nt single end reads on a HiSeq 2500 (Illumina) getting a minimum of 14 millions reads per sample, and dual-indexed libraries were sequenced 150 nt paired end reads on a NovaSeq 6000 (Illumina) getting a minimum of 25 millions reads per sample. qPCR was performed using SYBR Green I Master (Roche) kit using the primers in Supplementary Table S2. ChIP-seq data was mapped by Bowtie2 (43) to the genome build dm6 with a quality filter ≥10. Mapped reads of replicates were merged together and

BPM (bins per million) normalized. Peaks were identified by Macs3 and differential peaks were identified using the bdgdiff function using sequenced inputs for each sample/condition as a control (44). The normalized signal output of siQ-ChIP (45) was used to quantify widespread losses using peaks called in each sample. Elongation status was determined by RNAPII ChIP-seq from the pausing index calculated as previously described (11,46). Co-occupancy of CAP-H2 with various architectural proteins was calculated by the odds ratio of overlap and non-overlapping peaks from a previously created master list of architectural protein binding sites (26). Heatmaps and average profiles were generated by deeptools (47). Categorization of genes according to the levels of transcription was performed as described in (11). Briefly, genes without RNAPII were categorized by their lack of RNAPII ChIP-seq peak, while the pausing index (46) (defined by the ratio between the RNAPII ChIP-seq signal at the TSS +/- 500 bp and the rest of the gene body) was used to categorize elongating, mid-elongating, and paused genes according to standard deviation cutoffs around the mean.

In situ Hi-C library preparation

In situ Hi-C experiments were performed as previously described (48) with some modifications. Cross-linked cells were incubated for 30 min in ice in Hi-C lysis buffer (10 mM Tris–HCl at pH8, 10 mM NaCl, 0.2% NP-40), centrifuged for 5 min at 3500 g, resuspended in 190 µl of 1× NEBuffer2 (New England BioLabs [NEB]) and 10 µl of 10% SDS, and were then incubated for 10 min at 65°C. After the addition of Triton X-100 and 15-min incubation at 37°C, nuclei were centrifuged for 5 min at 3500g and were resuspended in 300 µl of 1× NEBuffer2. Nuclei were digested overnight using 400 U of the MboI restriction enzyme (NEB). For filling-in with bio-dATP, nuclei were pelleted and resuspended in fresh 1× repair buffer (1.5 µl of 10mM dCTP, 1.5 µl of 10 mM dGTP, 1.5 µl of 10 mM dTTP, 37.5 µl of 0.4 mM biotin-dATP, 50 U of DNA Polymerase I large [Klenow] fragment in 300 µl 1× NEBuffer2). Ligation was performed for 4 h at 16°C using 10 000 units of T4 DNA ligase (NEB) in 1.2 ml of ligation buffer (120 µl of 10 × T4 DNA ligase buffer, 100 µl of 10% Triton X-100, 12 µl of 10 mg/ml BSA, 963 µl of H_2O). After reversion of the cross-link, DNA was purified using phenol/chloroform/isoamyl. Purified DNA was sonicated to an average size of 300–400 bp using a Bioruptor (Diagenode; eight cycles of 20 s on and 60 s off), and 3 µg of sonicated DNA was used per *in situ* Hi-C library preparation. Briefly, biotinylated DNA was pulled down using 20 µl of Dynabeads MyOne T1 streptavidin beads in binding buffer (5 mM Tris–HCl at pH 7.5, 0.5 mM EDTA, 1 M NaCl). End-repair, A-tailing and Illumina adaptors ligation were performed on the beads using NEBNext library preparation end-repair and A-tailing modules (NEB). Libraries were amplified and sequenced in biological replicates, obtaining >200 million useable reads per condition after mapping, deduplication and merging replicates.

Hi-C data analysis

Sequenced reads were preprocessed, mapped to the *Drosophila* genome build dm6, filtered for quality score ≥10, and removed of PCR duplicates using HiC-Pro (49). After initial processing we obtained approximately 200 million useable contacts per condition (Supplementary Table S3), which is enough to resolve structural details of several layers of chromatin organization in the relatively small-sized *Drosophila* genome (27). Replicates were combined and the resultant maps were visualized with Juicebox (50). Distance normalization was calculated as the observed value compared to the average value at that distance in the formula (observed + 1)/(expected + 1). Percent inter-chromosomal interactions was calculated by the number of reads mapping to different chromosomes (e.g. chr2–chr3) versus mapping to the same chromosome (e.g. chr2–chr2, chr3–chr3, chr4–chr4, chrX–chrX). Compartments were identified by calculating the eigenvector on the Pearson correlation matrix in 10 kb bins as previously described (27). Saddle plots were created by sorting interactions by each anchor's eigenvector percentile (100 quantiles). Compartment strength was calculated by the average distance normalized signal within 5 quantiles in each category. TSS-TTS signal represents distance normalized Hi-C values in the 1 kb binned interaction overlapping the TSS and TTS. Topologically Associating Domains (TADs) were identified by insulation score at 1 kb resolution with the HiC1Dmetrics tool (51). Hi-C derived pairing (hd-pairing) profiles across the genome were identified from fragment-level orientation of ligation events in Hi-C as previously described and placed into 1 kb bins (11). Using the binned signal, hd-pairing peaks were identified under various FDR thresholds using the find_peaks tool: https://github.com/owenjm/find_peaks. Pc loops were identified by SIP and APA plots were generated by SIPMeta (52). Heatmap rows describing the hd-pairing signal at Pc-loop anchors were sorted according to the total signal across samples, and that same order was then used to calculate the running median of the distance from the Pc-loop anchor to a Z4 ChIP-seq peak. Allele-specificity of Pc-loop signal was derived by using the published 439 × 057 trans-homolog map in GSE121256 (12) in 5 kb bins and averaging the signal across loop anchors. Because the available published hybrid map was mapped to dm3, we converted the coordinates of Pc loop anchors using liftOver (53). Trans-homolog signal defining 'tight' pairing was evaluated similar to the original published report (12), in 5 kb bins and using the $\log_2$ ratio of inter-allele contacts vs. intra-allele contacts within a 30 kb window. Both hd-pairing and trans-homolog tracks were z-score normalized to allow their comparison.

ATAC-seq

ATAC experiments were performed as described (54). Briefly, nucleus were resuspended in 50 µl Tn5 transposase mixture (2.5 µl Tn5, 25 µl 2× TD buffer, 22.5 µl RNase Free Water), and incubated at 37°C for 30 min. After the reaction, the DNA was purified using the MinElute PCR Purification Kit (QIAGEN). The PCR cycles for the library preparation were determined by qPCR. Following amplification, the size selection of the library was performed using Ampure beads. The dual-indexed libraries were sequenced 50 nt paired end reads on a NovaSeq 6000 (Illumina) getting a minimum of 25 millions reads per sample. ATAC-seq data was trimmed of adapter sequences using cutadapt (55), aligned to the reference genome dm6 using bowtie2 (43), deduplicated with picard (https://broadinstitute.github.io/picard/), and peaks identified by macs2 with the extsize 147 and nomodel parameters (44).

Transposase hypersensitive sites (THSSs) and nucleosomes were separately analyzed by categorizing the reads by insert size (<120 bp versus 140–250 bp, respectively). Signal was BPM normalized and we tested for differential peaks by MANorm (56). Differential v-plots were created using NucleoATAC (57) at summits of Z4 peaks identified by macs2 (44).

Results

Z4 colocalizes with CAP-H2 and mediates its recruitment to APBSs *loci* for anti-pairing

From the multiple architectural proteins (APs) that decorate APBSs *loci*, CAP-H2 has the most prominent role in regulating pairing in *Drosophila* (7,11,26). To identify additional APs that could cooperate with CAP-H2 in the regulation of chromosome pairing, we analyzed ChIP-seq data for 16 other known APs. These analyses showed exceptionally high co-occupancy of CAP-H2 by Z4 (Figure 1A, Supplementary Figure S1A, B), even at sites showing low co-occupancy by other APs (APBS ⇐ 2) (Supplementary Figure S1C), indicative of a close association of CAP-H2 with Z4. Both Z4 and CAP-H2 preferentially localize at the TSS of transcriptionally active genes (Figure 1B). Co-immunoprecipitation experiments with αCAP-H2 antibodies further suggest the interaction between CAP-H2 and Z4 (Figure 1C). Interestingly, Z4/CAP-H2 binding sites highly overlap with binding sites for MRG15 (Supplementary Figure S1D), a protein that was previously shown to participate in the regulation of chromatin association of CAP-H2 (25,42).

Z4 is a C2H2 zinc-finger protein with potential DNA binding activity, suggesting that it might be involved in CAP-H2 recruitment. To test this possibility, we treated cells with dsRNA against Z4, which strongly decreased total Z4 protein levels (Supplementary Figure S1E). In comparison to control cells treated with dsRNA against LacZ, we observed that depletion of Z4 results in decreased CAP-H2 occupancy (Figure 1D). Using siQ-ChIP (45), we found that CAP-H2 peaks were globally reduced by approximately 2-fold and that there were no new CAP-H2 peaks in Z4 knockdown cells (Supplementary Figure S1F). ChIP-qPCR confirmed these results (Supplementary Figure S1G). Intriguingly, even though Z4 depletion results in the loss of CAP-H2 ChIP-seq peaks at APBSs *loci*, WB analysis of purified crosslinked chromatin showed no significant decrease in the levels of chromatin-bound CAP-H2 in Z4-depleted cells (Supplementary Figure S1H), suggesting that loss of Z4 impairs specific targeting of CAP-H2 to APBSs *loci,* without affecting its association with chromatin in a more general way, randomized within the population of cells.

CAP-H2 has a well-characterized anti-pairing function in *Drosophila* (7,11,26), and it was previously reported that CAP-H2 depletion increases pairing at APBSs *loci* bound by CAP-H2 (11). Thus, considering that Z4 depletion causes loss of CAP-H2 at APBSs *loci*, we anticipated that pairing would increase in Z4-depleted cells. To address this question, we performed Hi-C experiments and applied the hd-pairing method (11), which measures ligations between sequences from different chromosomes that result in the same digested fragment (Figure 1E). Using this metric, we observed that, indeed, Z4 knockdown cells show increased hd-pairing signal at Z4/CAP-H2 binding sites (Figure 1F and G). Pairing strongly correlates with CAP-H2 occupancy (11,12) (Supplementary Figure S2A) and, in fact, the impact of Z4 knockdown on pairing is more dramatic at APBSs *loci* with higher CAP-H2 occupancy (Figure 1H). Similar results were obtained by fluorescence *in situ* hybridization (FISH). In these experiments, we determined pairing at the heterochromatic AACAC and 359 *loci*, which are known to be regulated by CAP-H2 (21), and found increased pairing in Z4-depleted cells (Figure 1I). In fact, while hd-pairing signal at AACAC *locus* could not be determined due to its highly repetitive sequence, hd-pairing signal at the 359 *locus* was found to increase after Z4 knockdown (Supplementary Figure S2B). Altogether these results suggest that Z4 and CAP-H2 cooperate to negatively regulate pairing.

It was previously noted that pairing occurs in active/accessible regions of the genome that show high ATAC-seq signal (12,14). Thus, we tested if loss of Z4, and consequently CAP-H2, alters chromatin accessibility at APBSs *loci*. We performed paired-end ATAC-seq, that, based on the fragment sizes, helps identify and analyze separately nucleosome vs. Tn5 hypersensitive sites (THSS), at which TF's may be bound (57,59) (Supplementary Figure S3A). Interestingly, we found that pairing was higher at Z4 occupied ATAC-seq peaks compared to non-Z4 peaks (Supplementary Figure S3B), which is consistent with stronger pairing at Z4/CAP-H2 sites. Regardless, we observed that ATAC-seq signal was high at APBSs *loci* in control LacZ cells with little to no change after Z4 depletion (Supplementary Figure S3C), except for a slight decrease of THSS fragments centered at Z4 ChIP-seq peaks (Supplementary Figure S3D and E), which likely reflects the relationship of THSS signal with the binding of regulatory proteins (54,60). These results suggest that increased pairing detected at APBSs *loci* upon Z4 depletion does not correlate with large widespread changes to chromatin accessibility.

Altogether these results indicate that Z4 cooperates with CAP-H2 to promote chromosome unpairing. CAP-H2 is a subunit of condensin II, a multisubunit complex essential in regulating chromosome condensation in both *Drosophila* and vertebrates (9,25,61–63); thus, we asked if Z4 depletion also affects chromatin condensation. It has been shown that, in *Drosophila*, CAP-H2 depletion impairs chromosome condensation in interphase, resulting in a significant 15%-20% increase of nuclear volume (9,62). In this regard, though not statistically significant, we detect a slight 8% increase in the nuclear volume of Z4 knockdown cells (Supplementary Figure S4A). Impaired condensin II function has also been shown to affect condensation of mitotic chromosomes. In chicken DT40 cells depletion of the CAP-D3 subunit results in strong disorganization of mitotic chromosomes that lose their normal morphology (63). However, in *Drosophila,* depletion of CAP-H2 has weaker effects, affecting axial compaction of mitotic chromosomes while preserving their overall structure (25,61). In this regard, we observed that, while the morphology of mitotic chromosomes is largely preserved in Z4-depleted cells (Supplementary Figure S4B), chromatid length increases weakly in Z4-depleted cells (Supplementary Figure S4C), indicating a partial defect on axial compaction. Concomitantly, chromatids were thinner upon Z4 depletion (Supplementary Figure S4D). Altogether these results suggest that Z4 depletion partially affects chromatin condensation without causing gross condensation defects.

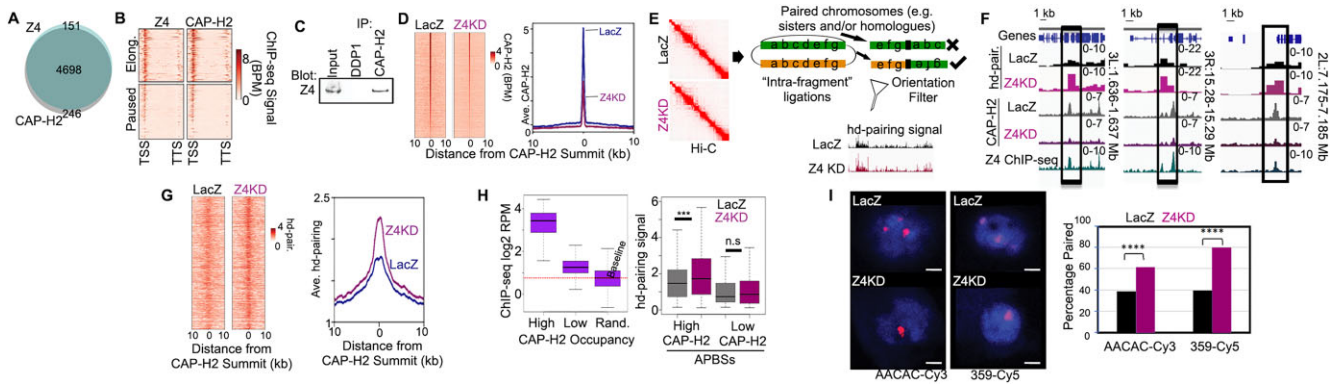

Figure 1. Z4 mediates CAP-H2 recruitment to APBSs *loci* to control chromosome pairing. (**A**) Venn diagram displaying the overlap between Z4 and CAP-H2 ChIP-seq peaks. (**B**) Heatmap of ChIP-seq signal for Z4 and CAP-H2 at genes. (**C**) Co-immunoprecipitation of Z4 with αCAP-H2 antibodies. IP with unrelated αDDP1 antibodies are shown as control. (**D**) Heatmap (left) and average profile (right) of CAP-H2 ChIP-seq signal in control LacZ and Z4KD cells. (**E**) Schematic representation of how the hd-pairing method uses fragment-level oriented ligation events in Hi-C, and removal of possible self-circularizations, as a sequencing-based measure of pairing interactions. (**F**) Example *loci* showing the hd-pairing signal and CAP-H2 ChIP-seq signal in control LacZ and Z4KD cells. Z4 ChIP-seq signal in control LacZ cells is shown to highlight the overlap with CAP-H2. (**G**) Heatmap (left) and average profile (right) of hd-pairing signal in control LacZ and Z4KD cells at CAP-H2 peaks. (**H**) Left: average CAP-H2 ChIP-seq signal at APBSs *loci* categorized as of high ($n = 6247$) and low ($n = 11\,559$) CAP-H2 occupancy. The background CAP-H2 ChIP-seq signal is also shown. Right: hd-pairing signal in control LacZ and Z4KD cells at APBSs *loci* that have high versus low CAP-H2 ChIP-seq signal. *** indicates *P*-value < 2.2e-16 and n.s. is not significant ($P = 0.056$); Wilcoxon Rank Sum test. (**I**) FISH analysis in control LacZ and Z4KD cells with probes for the AACAC and 359 *loci* (in red). DNA was stained with DAPI (in blue). Scales bars correspond to 5 μm. Right: Percentage of cells where the *loci* were paired. Results are the sum of three independent experiments showing similar results. $n = 226$ and 184 for AACA-Cy3 in control LacZ and Z4KD cells, respectively; $n = 195$ and 181 for 359-Cy5 in control LacZ and Z4KD cells, respectively. **** indicates *P*-value < .0001; two tailed Fischer exact test.

Hyperosmotic stress disrupts chromosome pairing in a Z4-dependent manner

Chromatin is highly responsive to stressors, and stress conditions can be used as a tool to gain mechanistic insights into 3D chromatin organization (34,35,64). In particular, hyperosmotic stress has been shown to induce rapid and reversible changes to 3D chromatin organization in human cells (34). However, if osmostress has similar effects in other species and whether chromosome pairing is affected is not known. To address these questions, we performed Hi-C experiments in *Drosophila* cells subjected to NaCl-induced hyperosmotic stress and after recovery in isotonic conditions (Figure 2A). After hyperosmotic stress, Hi-C contact maps display visible changes in contact intensity (Figure 2A), which correspond to increased long-range (off-diagonal) signal (Supplementary Figure S5A). The increased interaction range may be due to the known decrease in nuclear size (Supplementary Figure S5B) (33), thereby constricting the physical space of chromatin. Consistent with this, osmostress resulted in increased inter-chromosomal (e.g. chr2-chr3) interactions (Supplementary Figure S5C and S5D), suggesting that chromosome territories are less distinct. After recovery from osmostress, the interaction distance profiles reverted to what was seen in isotonic conditions (Figure 2A and Supplementary Figure S5A), and inter-chromosomal interactions decreased to normal levels (Supplementary Figure S5C and S5D). These results suggest that, like previously reported in mammalian cells (34), osmostress induces acute and reversible broad-scale changes to chromatin architecture in *Drosophila* cells.

Next, we analyzed the effects of osmostress on chromosome pairing. In these experiments, we used both control LacZ and Z4-depleted cells. In control LacZ cells, we observed a widespread loss of hd-pairing at APBSs *loci* that was almost fully restored after recovery from osmostress (Figure 2B and C), suggesting that osmostress induces fast and reversible chromosome unpairing. Next, we analyzed the effects in Z4-depleted cells that, as mentioned above, show increased chromosome pairing in isotonic conditions (Figure 1G). We observed that, like in control LacZ cells, osmostress decreased pairing in Z4-depleted cells (Figure 2B and D). However, while osmostress results in a nearly complete loss of pairing in control LacZ cells (Figure 2B and C), hd-pairing was still high in Z4 knockdown cells, even to a level that was similar to what is found in control LacZ cells under isotonic conditions (Figure 2B and D). This incomplete unpairing in Z4 knockdown cells indicates that loss of pairing during hyperosmotic stress is mediated through Z4. In addition, we observed that, while hd-pairing is unable to fully recover after stress release in control LacZ cells (Figure 2B, C and E), pairing is restored to a higher amount than original levels in Z4 knockdown cells (Figure 2B, D, and E), indicating that loss of Z4 allows pairing sites to more robustly reassert themselves. Altogether these results suggest that Z4 regulates the loss of pairing during osmostress and its recovery upon stress release. Interestingly, we observed that the changes induced by osmostress in control LacZ cells are stronger at APBSs *loci* with high CAP-H2 levels than at sites showing low CAP-H2 occupancy (Figure 2F), suggesting that chromosome unpairing in osmostress, which depends on Z4, also depends on CAP-H2, which is consistent with the cooperation of Z4 and CAP-H2 in pairing regulation.

Osmostress impairs localization of APs and reduces RNAPII occupancy at APBSs *loci*

Results reported above suggest that loss of chromosome pairing could be due to increased association of Z4/CAP-H2 with chromatin. However, western blot (WB) analyses after crosslinking and purification of chromatin found no difference in the levels of chromatin-bound Z4 or CAP-H2 after osmostress (Figure 3A). ChIP-seq and ChIP-qPCR experiments showed a surprising widespread loss of ChIP-seq peaks for both Z4 and CAP-H2 after osmostress (Figure 3B,

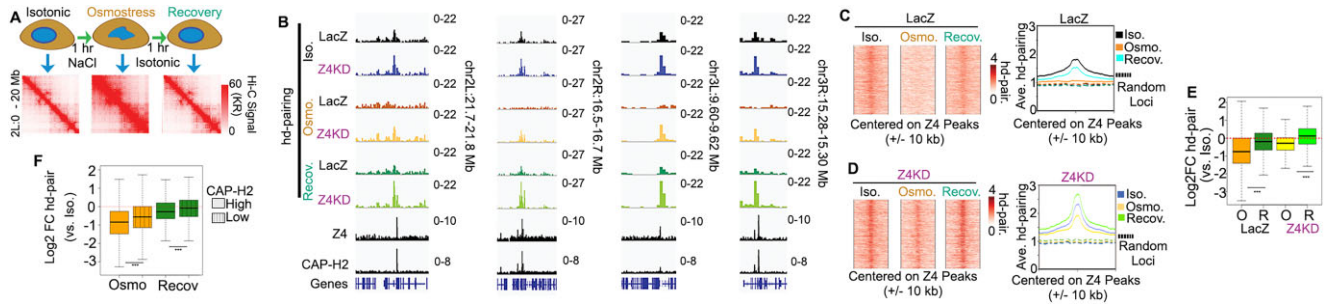

Figure 2. Hyperosmotic stress disrupts chromosome pairing in a Z4-dependent manner. (**A**) Overview of experimental design including hyperosmotic stress conditions along with recovery in isotonic media. (**B**) Example *loci* showing the hd-pairing signal under isotonic, osmostress, and recovery conditions in control LacZ and Z4KD cells. CAP-H2 and Z4 ChIP-seq signals in control LacZ cells are also shown. (**C, D**) Heatmaps (left) and average profiles (right) of hd-pairing signal at Z4 peaks under isotonic, osmostress, and recovery conditions in control LacZ (**C**) and Z4KD cells (**D**). Dashed lines represent the average hd-pairing signal in each condition at random *loci*. (**E**) The $\log_2$ fold change in hd-pairing signal at APBSs *loci* ($n = 17\,806$) relative to isotonic conditions is shown for control LacZ and Z4KD cells in osmostress and recovery conditions. Boxes represent the median and interquartile range (IQR), whiskers are 1.5 * IQR. The red dashed line is at zero to indicate no change from isotonic conditions. *** indicates *P*-value < 2.2e-12; Wilcoxon Rank Sum test. (**F**) As in **E**, but for APBSs *loci* with high ($n = 6247$) versus low ($n = 11\,559$) CAP-H2 levels in control LacZ cells. *** indicates $P < 2.2e\text{-}12$ (left) and $P = 2.339e\text{-}8$ (right); Wilcoxon Rank Sum test.

and Supplementary Figure S6A). Altogether, these results suggest that, Z4 and CAP-H2 remain associated with chromatin during osmostress but lose their target specificity. This delocalization was unexpected, considering that Z4 and CAP-H2 are anti-pairers and that chromosome unpairing after osmostress depends on Z4. Thus, we hypothesized that osmostress could affect the structural organization of APBSs *loci* in a more general way. Indeed, assaying BEAF-32, another well-known AP, we observed a similar delocalization from APBSs *loci* (Supplementary Figure S6B and C), despite general retention on the crosslinked chromatin (Supplementary Figure S6D). APBSs *loci* overlap transcriptionally active genomic sites (12,14) and are often occupied by RNAPII. Therefore, to test if osmostress affects RNAPII localization at APBSs *loci*, we performed RNAPII ChIP-seq experiments in both control LacZ and Z4 knockdown cells. In isotonic conditions, RNAPII ChIP-seq peaks are overall maintained at the same *loci*, with a slight decrease of signal in Z4 knockdown compared to LacZ cells (Figure 3C and D). Similarly, we observed that osmostress caused decreased signal, but did not cause a global complete loss of RNAPII ChIP-seq peaks (Figure 3C), which is in sharp contrast to the complete loss of Z4, CAP-H2, and BEAF-32 ChIP-seq peaks observed upon osmostress (Figure 3B and Supplementary Figure S6A–C). Furthermore, we found that the majority of osmo-sensitive RNAPII peaks in control LacZ cells, were also osmo-sensitive in Z4 knockdown cells (Figure 3E). Most remarkably, we found that osmo-sensitive RNAPII sites were occupied by Z4 and CAP-H2, as well as by many other APs, indicating that they correspond to APBSs *loci* (Figure 3F). Consistent with this, osmo-sensitive RNAPII *loci* had high hd-pairing signal in isotonic conditions (Figure 3F), which is lost after osmostress in control LacZ cells and strongly decreased, but not abolished, in Z4 knockdown cells (Figure 3F). Altogether these results indicate that osmostress specifically reduces RNAPII occupancy at APBSs *loci*, suggesting a correlation between reduced RNAPII occupancy and loss of pairing during osmostress. Interestingly, no such correlation is observed in the case of Z4 depletion since, despite increased pairing, we observed that a large proportion of osmo-sensitive RNAPII peaks also decrease after Z4 depletion in isotonic conditions (Figure 3G), albeit to a lesser degree (Figure 3H). Therefore, Z4 depletion in isotonic conditions leads to increased pairing, but decreased RNAPII occupancy at APBSs *loci*.

Chromosome pairing interactions correlate with the strength of intra-chromosomal 3D interactions

Next, taking advantage of the opposite effects that Z4 depletion and osmostress have on chromosome pairing, we examined the possible correlation between inter-chromosomal pairing interactions and other layers of 3D chromatin organization. For this purpose, we used Hi-C data obtained from control LacZ and Z4-depleted cells under isotonic and osmostress conditions, as well as after recovery from osmostress.

We identified compartments at 10 kb resolution by principal component analysis (PCA), the resultant eigenvector denoting A and B compartments corresponding to active and inactive regions, respectively (1,27,65). As previously reported, we found higher pairing signal in A compartments (Supplementary Figure S7A) (11), which decreased in control LacZ cells in osmostress conditions. We see opposite effects in the B compartment intervals, but the overall level of pairing remained lower than what was found in the A compartment under isotonic conditions (Supplementary Figure S7A). In contrast to their impacts on pairing, we found that the identity of compartments remained fairly unchanged between all the different conditions (Supplementary Figure S7B and C). Although intervals did not change compartment identity, A-A interaction intensity was weaker in osmostress, an effect which is partially counteracted in Z4-depleted cells (Figure 4A). We also examined TADs, the borders of which in *Drosophila* overlap both compartmental boundaries and APBSs *loci* (27) and found a slight weakening of insulation upon osmostress (Supplementary Figure S7D).

Next, we examined the chromatin organization of genes, which were previously shown to have high intra-genic interactions and form contacts between the transcription start site (TSS) and the transcription termination site (TTS), otherwise known as gene-loops (11,27,66–68). In *Drosophila*, intragenic gene-loop interactions correlate with transcription elongation (11). We categorized genes by RNAPII ChIP-seq pausing index and, indeed, we detected higher intragenic gene-loop interactions on elongating and mid-elongating genes compared

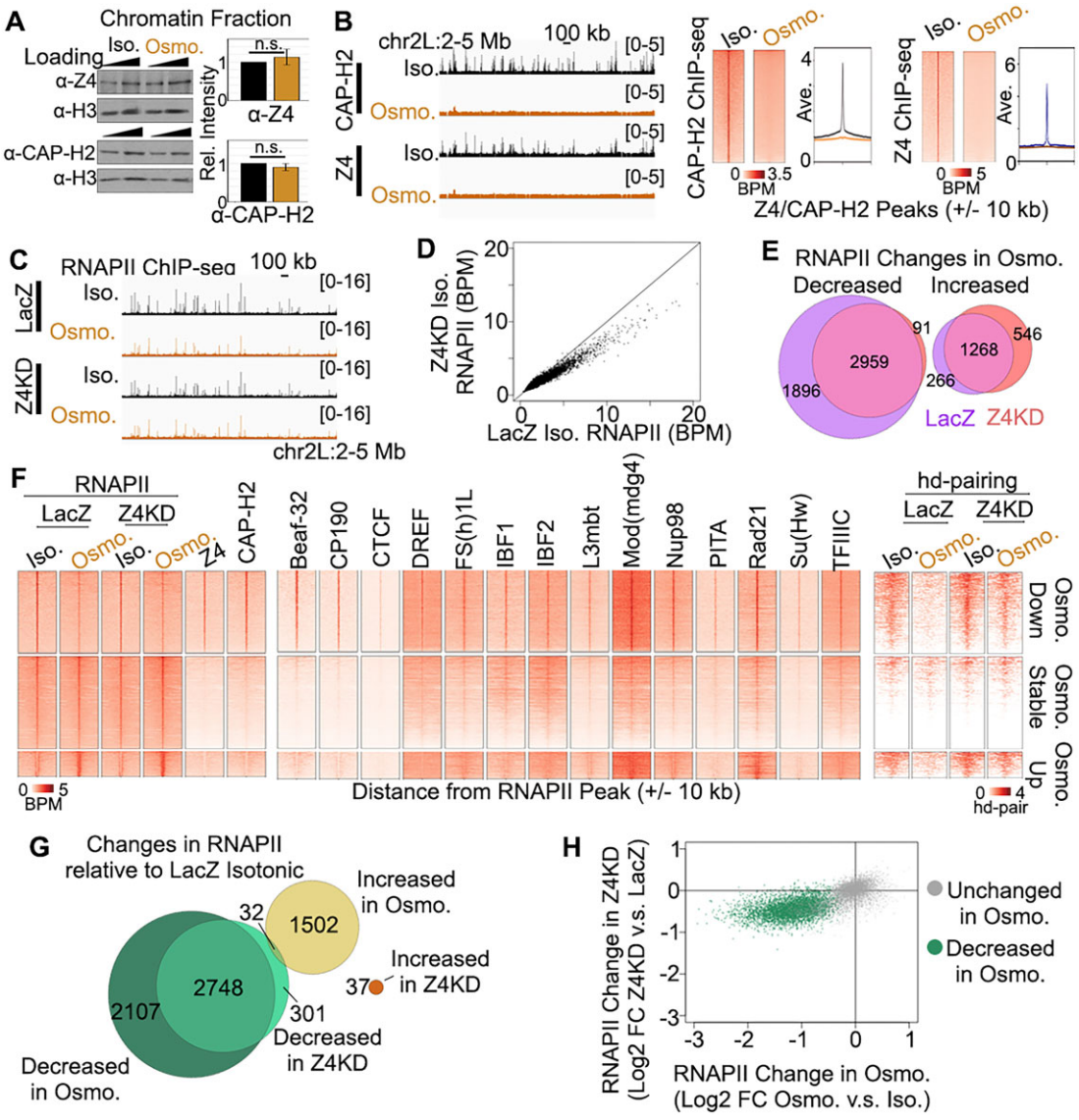

Figure 3. Hyperosmotic stress induces delocalization of APs from APBSs *loci* and decreased RNAPII. (**A**) WB (left) and quantification (right) of chromatin-bound Z4 and CAP-H2 levels in control LacZ cells under isotonic and osmostress conditions. Increasing amounts of purified crosslinked chromatin are shown. H3 is shown as loading control and quantification of bands is normalized by H3 levels. Results are the average of three independent experiments. Error bars are S.D.. *P*-values > 0.05; two-tailed Student's *t*-test. (**B**) Left: CAP-H2 and Z4 ChIP-seq tracks showing widespread loss of peaks in osmostress. Right: Heatmaps and average profiles of ChIP-seq signal for CAP-H2 and Z4 in isotonic and osmostress conditions. (**C**) RNAPII ChIP-seq tracks in control LacZ and Z4KD cells under isotonic and osmostress conditions. (**D**) RNAPII ChIP-seq signal at RNAPII ChIP-seq peaks in LacZ (x-axis) versus Z4KD (y-axis) cells in isotonic conditions. Diagonal line represents values where peaks without change would lie. (**E**) The overlap between RNAPII ChIP-seq peaks that changed after osmostress in control LacZ (purple) and Z4KD (peach) cells. (**F**) Heatmap for the RNAPII ChIP-seq signal in control LacZ and Z4KD cells under isotonic and osmostress conditions is shown at sites categorized by the changes in RNAPII occupancy after osmostress in control LacZ cells. ChIP-seq signals for the indicated APs in control cells under isotonic conditions are also shown. hd-pairing signal in control LacZ and Z4 KD cells under isotonic and osmostress conditions is also shown. (**G**) The overlap of RNAPII peaks of control LacZ cells changing after osmostress and upon Z4 depletion in isotonic conditions. (**H**) The log2 fold-change (FC) in RNAPII ChIP-seq signal at RNAPII ChIP-seq peaks of control LacZ cells after Z4 depletion in isotonic conditions (y-axis) is plotted against the log2 FC after osmostress (x-axis).

to paused genes and genes without RNAPII (noRNAPII) (Figure 4B and C). We observed that, concomitant to reduced pairing (Figure 2), intragenic gene-loop interactions were decreased under hyperosmotic stress (Figure 4B and C, and Supplementary Figure S7E), an effect which was partially counteracted in Z4-depleted cells (Figure 4B and C). Notably, concomitant to increased pairing (Figure 1F–I), Z4 depletion resulted in increased interactions between the 5′ and 3′ ends of genes compared to the gene-body (Figure 4B and Supplementary Figure S7F), which matches with the location of Z4/CAP-H2 at the TSS of genes (Figure 1B).

To analyze the correlation between chromosome pairing and intragenic gene-loop interactions, we directly measured hd-pairing at genes. Remarkably, we found that hd-pairing signal was high at the TSS of active genes (either elongating, mid-elongating or paused), while no hd-pairing signal was detected at noRNAPII genes (Figure 4D). We also noticed that hd-pairing signal was localized primarily to the

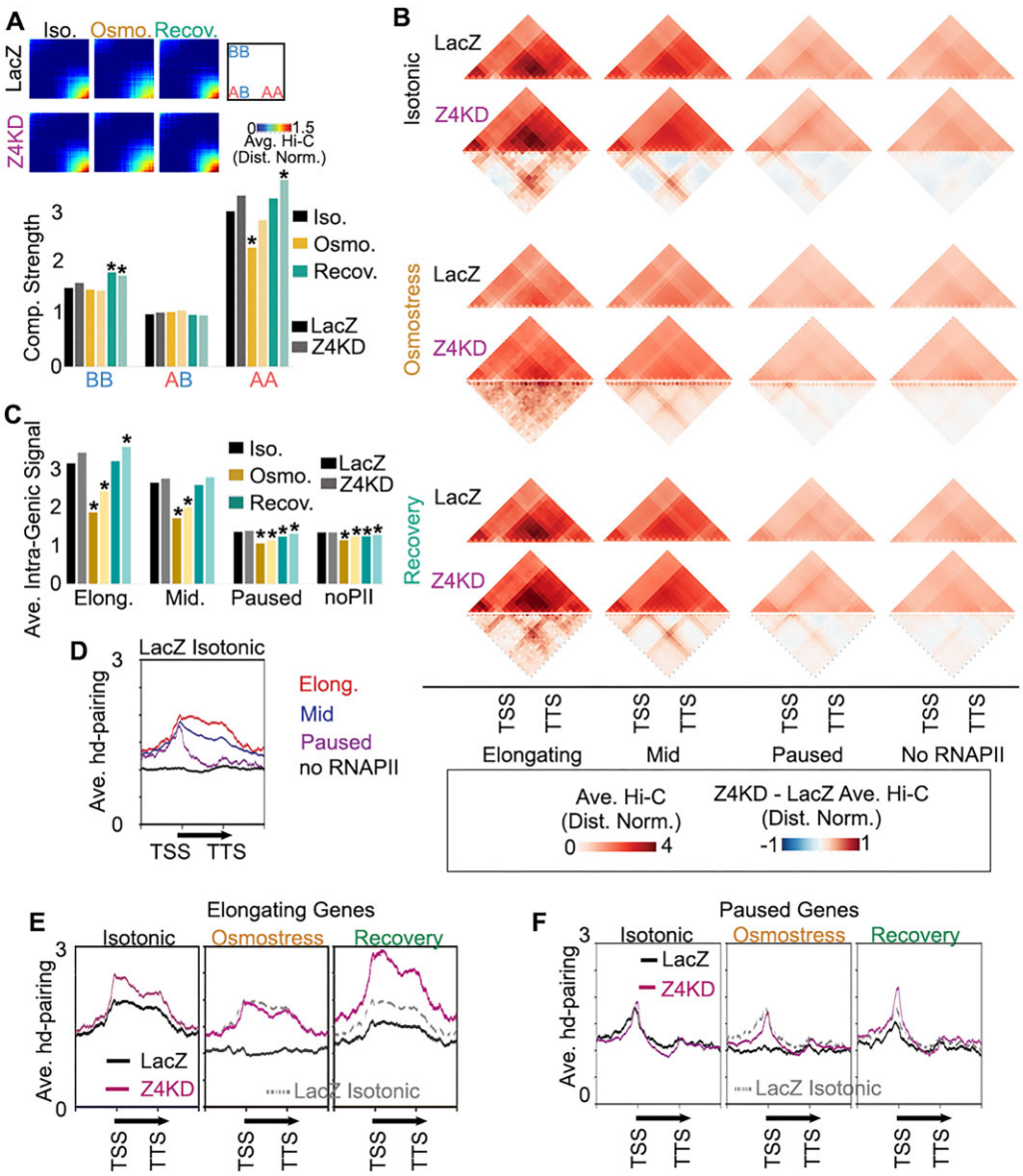

Figure 4. Chromosome pairing correlates with AA and intragenic gene-loop interactions. (**A**) Top: saddle plot analysis of compartments in control LacZ and Z4KD cells under isotonic, osmostress, or recovery conditions. Bottom: Compartment strength quantification from saddle analysis. * indicates bonferonni adjusted $P < .05$ from the Dunn's test between the respective saddle quadrants of all conditions relative to control LacZ cells under isotonic conditions. Bars without * were not significant. (**B**) Average distance normalized Hi-C signal in control LacZ and Z4 KD cells under isotonic (top), osmostress (center), and recovery (bottom) conditions at genes categorized by the RNAPII pausing index into elongating, mid-elongating, paused and without RNAPII (noRNAPII). Average difference in intragenic interactions in Z4KD compared to control LacZ cells is also shown. (**C**) Quantification of intragenic gene–loop interactions show in (**C**). * indicates bonferonni adjusted $P < 0.05$ from the Dunn's test of the average intragenic signal between all conditions relative to control LacZ cells under isotonic conditions. Bars without * were not significant. (**D**) Average hd-pairing signal in control LacZ cells under isotonic conditions for genes categorized by the pausing index. (**E, F**) Average hd-pairing signal at elongating (**E**) and paused (**F**) genes in control LacZ and Z4KD cells under isotonic, osmostress, and recovery conditions. Average hd-pairing signal in control cells under isotonic conditions (gray dashes) is also shown for comparison.

TSS of paused genes but extended into the bodies of elongating and mid-elongating genes (Figure 4D). Noteworthy, in response to osmostress and Z4 depletion, hd-pairing across elongating and mid-elongating genes followed the same general trends described above (Figure 2), namely it strongly decreases in control LacZ cells under osmostress conditions, an effect which is counteracted in Z4-depleted cells (Figure 4E and Supplementary Figure S7G). Interestingly, we observed that depletion of Z4 resulted in increased hd-pairing both at the TSS and throughout the body of elongating genes in isotonic conditions (Figure 4E), suggesting that, despite being preferentially bound to the TSS (Figure 1B), Z4 depletion impacts pairing interactions all across the gene-body. In contrast, only small changes in pairing were detected at paused genes which have lower Z4 levels and for which hd-pairing and differences between conditions are largely constrained to the TSS (Figure 4F). Lastly, genes lacking RNAPII do not show enrichment of hd-pairing signal (Figure 4D) and we detected no change in any of the conditions (Supplementary Figure S7H). Altogether these results illustrate pairing at the gene level and unveil its strong correlation with intragenic gene-loop interactions, particularly at active elongating genes.

Chromosome pairing reinforces Pc-loop interactions

Next, we analyzed the possible correlation of chromosome pairing with the strength of punctate chromatin loops anchored by Polycomb (Pc) (26,29,30) (Figure 5A). We observed that Pc-loop anchors are not enriched in Z4/CAP-H2 binding (Figure 5B) and, in fact, hd-pairing signal at Pc-loop anchors is generally low (Figure 5C). When we examined the distance to nearby Z4 peaks, we found that Pc-loop anchors closer to a Z4 peak showed higher hd-pairing signal than anchors further away from a Z4 peak (Figure 5D). We therefore categorized Pc-loops by hd-pairing signal at the anchors and found that, intriguingly, Pc-loops with higher pairing had higher Hi-C loop signal (Figure 5E). Noteworthy, we observed that depletion of Z4 increased pairing at Pc-anchors (Figure 5C and D) and, concomitantly, the strength of Pc-loop interactions increased both at highly paired and lowly paired Pc-loops (Figure 5E). These results suggest a correlation between Pc-loop intensity, pairing, and proximity to a Z4/CAP-H2 peak, such that nearby pairing could reinforce Pc-loop interactions. An example of this is shown in Figure 5A, where a Pc-loop is flanked by pairing sites that increase hd-pairing signal upon Z4-depletion (Figure 5A, highlighted in blue), and the intensity of the Pc-loop changes accordingly (Figure 5A). Notice that, in this case, despite the sites of pairing are also bound by Pc, it is not directly involved in loop formation (Figure 5A), suggesting that pairing helps strengthen Pc-loops, but is insufficient for their formation.

To analyze further the possible contribution of chromosome pairing to Pc-loop interactions, we examined published haplotype resolvable Hi-C data in a *Drosophila* hybrid cell line (12). While the number of read-pairs after haplotype filtering was insufficient for the hd-pairing algorithm (see Discussion), we found that sites with hd-pairing signal in Kc167 cells corresponded to tight inter-homolog interactions in the hybrid cell line (Figure 6A and B). This suggests that pairing buttons are at least partially conserved, and that hd-pairing mostly detects the previously described tight pairing interactions (12). We then performed a 5 kb resolution analysis of Pc-loops (Figure 6C). Intriguingly, we detected Pc-loop signal on each allele as well as on the map of inter-allele interactions (Figure 6C). We then examined loops categorized by high v.s. low pairing (Figure 5D) and found that Pc-loops with high pairing had higher loop signal in both the intra-allele and inter-allele maps (Figure 6D), suggesting that pairing may contribute to both types of interactions. Notably, at highly-paired Pc-loops, the inter-allele signal was more similar to the intra-allele signal (Figure 6E). In contrast, at low-paired Pc-loops, the inter-allele signal was lower than the intra-allele signal (Figure 6E). These results show high inter-allele Pc-loop interactions, and a correlation between Pc-loop intensity and pairing level, indicating that pairing likely contributes to the intensity of Pc-loops as measured by Hi-C (12).

Discussion

Here, we have analyzed somatic chromosome pairing in *Drosophila*, a model system in which chromosomes undergo robust pairing throughout interphase in somatic cells (7,9,10). To analyze chromosome pairing we have used hd-pairing (11), a Hi-C based methodology that infers pairing from the frequency of oriented ligation events between fragments of identical sequence and, consequently, measures tight pairing interactions without taking into account loose pairing interactions that involve non-identical fragments in a 'register shifted' manner (12,14). It must be noted that hd-pairing does not formally distinguish sister chromatid pairing from homologue pairing. Currently, it remains unclear whether sisters and homologues pair through the same *loci* and mechanisms. In principle, it would be possible to use hd-pairing in conjunction with haplotype-resolvable Hi-C data (12,14) to answer these questions. However, using the deepest published haplotype-resolvable Hi-C data that has >500 million usable contacts (12), we obtained only approximately 13 000 useable reads per condition after allelic assignment, which filters >4/5th of the reads and hd-pairing, which examines only intra-fragment ligations. Therefore, hd-pairing analysis of haplotype-resolved sequencing data will require to increase current sequencing depths by, at least, 50-fold to approximately 25 billion reads. Nevertheless, use of hd-pairing in G1 cells demonstrated that it can detect homologue pairing (11). Moreover, by comparing hd-pairing data in asynchronous Kc167 cells with haplotype-resolvable Hi-C data in a hybrid cell line, our results suggest that hd-pairing mostly detects tight inter-homologue pairing interactions.

In *Drosophila*, tightly paired *loci* correspond to APBSs (11–15,17), where a large number of APs bind. Chromosome pairing results from the balance between opposing pairing and anti-pairing activities (7) and, although multiple factors have been reported to influence pairing (21), only a few correspond to known APs that might be directly involved in pairing interactions with CAP-H2's role in anti-pairing being the most widely studied (7,9–11,23–25). The difficulty in identifying other proteins involved in pairing may be related to the proposed cooperative role of APs (11,15,17,19). Here, we identify the zinc-finger protein Z4, a well-known AP, as a regulator of CAP-H2 localization and anti-pairing activity at APBSs *loci*. Z4 interacts with CAP-H2 and binds to the same *loci*, while depletion of Z4 causes loss of CAP-H2 occupancy at APBSs *loci* and increases tight pairing interactions. From our results, it cannot be determined if Z4 also impacts 'loose' pairing interactions. However, a previous report found that knockdown of Slmb, which causes increased CAP-H2 levels, affects tight but not 'loose' pairing interactions (12). It is somewhat surprising that, despite their anti-pairing activity, APBSs *loci* bound by Z4/CAP-H2 show strong pairing that, in fact, is higher than at sites lacking Z4/CAP-H2. These observations likely reflect the highly dynamic nature of pairing interactions and suggest that Z4/CAPH-2 target tightly paired sites to prevent excess pairing. Interestingly, Z4 depletion does not affect the global level of chromatin-bound CAP-H2, suggesting that Z4 is required to specifically target CAP-H2 to APBSs *loci* and that, in the absence of Z4, CAP-H2 binds chromatin in a more general not-target specific way, randomized within the population of cells. MRG15 has also been reported to be involved in CAP-H2 recruitment to chromatin (25,42). Although the direct role of MRG15 in CAP-H2 binding at APBSs *loci* has not been determined, our results show that it highly overlaps with Z4/CAP-H2, suggesting a functional cooperation. It is possible that, together with CAP-H2, Z4 depletion induces MRG15 delocalization, which could still mediate chromatin binding of CAP-H2. Future work will clarify these questions. Here we have also shown that osmostress induces fast and reversible chromosome unpairing in a Z4/CAP-H2-dependent manner. It was previously shown that, in mammalian cells, osmostress alters intra-chromosomal 3D interactions (34), but the effects on inter-chromosomal pairing interactions were not

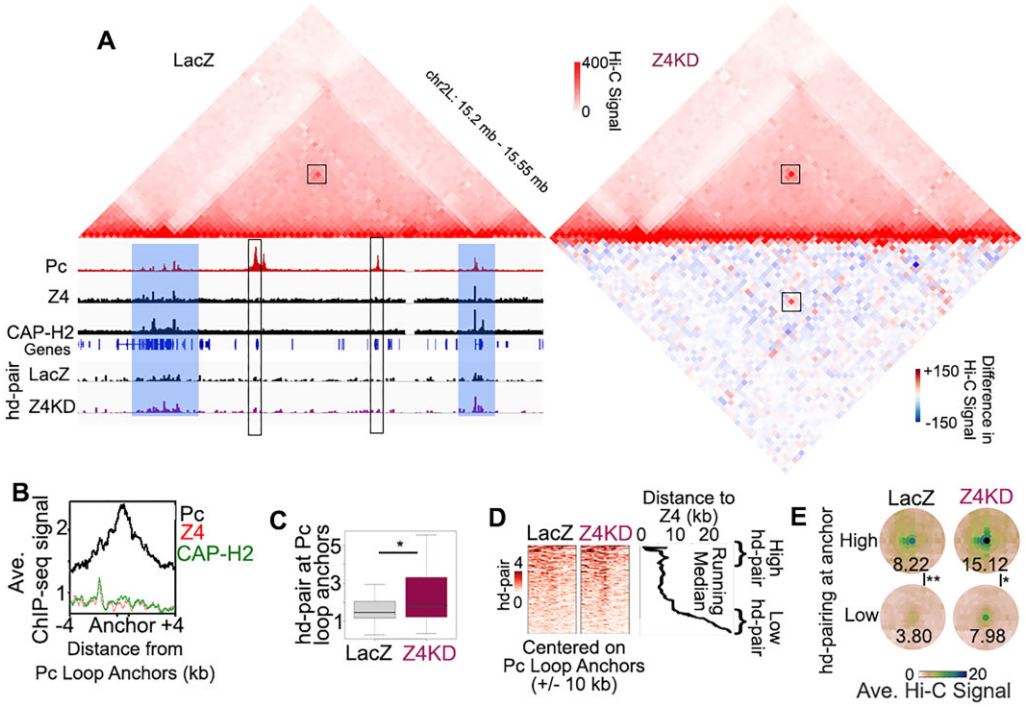

Figure 5. Chromosome pairing reinforces Pc-loop interactions. (**A**) Example of a Pc loop in control LacZ and Z4KD cells. Pc, Z4 and CAP-H2 ChIP-seq signals in control cells are shown to highlight the overlap of Pc, but not Z4/CAP-H2 at these loop anchors. hd-pairing signal is shown below to highlight the nearby peaks of pairing (highlighted in blue) that increases in Z4KD cells. (**B**) Average ChIP-seq signal for Pc, Z4 and CAP-H2 at 1 kb Pc loop anchors. (**C**) Boxplot of hd-pairing signal at Pc-loop anchors in LacZ (grey) and Z4KD (maroon) cells. * indicates $P < .05$; Wilcoxon Rank Sum test. (**D**) Left: Heatmap of hd-pairing at Pc-loop anchors in control LacZ and Z4KD cells. Right: profile of the distance from Pc-loop anchor to the closest Z4 ChIP-seq peak. *Loci* at the top and bottom of the heatmap were categorized as high and low hd-pairing in downstream analysis. (**E**) Average distance normalized Hi-C signal in control LacZ and Z4KD cells at Pc-loops categorized as highly-paired or lowly-paired. APA scores for each condition are indicated. ** $P \leq 0.01$; * $P \leq 0.05$ Monte Carlo permutation testing.

known. The dramatic loss of pairing induced by osmostress is somewhat surprising given the reduced nuclear volume and increased chromatin condensation observed under osmostress conditions (31–33). In this regard, our results show that osmostress strongly affects the molecular organization of APBSs *loci*, inducing delocalization of APs without affecting their total chromatin-bound levels. Delocalization of APs from APBSs *loci* is consistent with previous reports showing reorganization of APs upon osmostress (31). On the other hand, our results show that loss of hd-pairing coincides with a general gain in total inter-chromosomal interactions in osmostress. Altogether these results suggest that osmostress results in loss of specific pairing interactions at APBSs *loci* and increased non-specific intermingling of all chromosomes. Loss of specific localization of APs at APBSs *loci* without affecting their total chromatin-bound levels, could reflect a randomization of binding, and perhaps pairing, within the cellular population making them not detectable by bulk genomic experiments (e.g. ChIP-seq and Hi-C), which average across the population. Osmostress could impact multiple biophysical and biochemical processes, but the fact that osmostress-induced unpairing depends on Z4/CAP-H2 suggests that it is likely an active process. In this regard, loss of Z4 and CAP-H2 at APBSs *loci* in osmostress was surprising, yet supports the hypothesis that anti-pairers target paired sites and become unbound after unpairing (11). Parallel to loss of pairing, osmostress decreases RNAPII occupancy at APBSs *loci*. This decrease occurs specifically at APBSs *loci* since RNAPII occupancy at most other sites is unaffected, and, even in some cases, is increased. Decreased RNAPII occupancy at APBSs *loci* likely reflects decreased transcription. In this regard, a role of transcription and RNA-mediated phase separation in chromosome pairing has been proposed (69). It is tempting to speculate that, to some extent, osmostress impairs transcription-mediated pairing by altering the biophysical properties of phase-separated chromatin condensates. Further work will answer these questions.

Our results also highlight the correlation between inter-chromosomal pairing interactions and intra-chromosomal 3D interactions. We show that Z4 depletion, and therefore loss of CAP-H2, increases pairing and reinforces AA and intragenic gene-loops interactions. On the opposite, osmostress abolishes pairing and, concomitantly, the strength of AA and gene-loop interactions strongly decrease. The interplay between pairing and intra-chromosomal 3D interactions is also demonstrated by the correlation between Pc-loop signal intensity and the proximity to Z4/CAP-H2 peaks. In this case, pairing propagates from Z4/CAP-H2 sites to proximal Pc-loops and, despite Z4/CAP-H2 are not directly enriched at the anchors, Z4 depletion affects Pc-loop signal. Our finding that Pc-loop signal is also inter-allelic in haplotype-resolved Hi-C also provides evidence that is in favor of the contribution of pairing to Pc-looping. Similarly, Z4/CAP-H2 localize at the TSSs of elongating genes, yet Z4 depletion increases pairing all across the gene body, and not only at the TSS. Thus, by combining Z4 depletion and osmostress, our results support a contribution of chromosome pairing to other features of 3D chromatin organization. However, we cannot exclude the possibility that, rather than to chromosome pairing, the observed effects on 3D chromatin organization are due to changes in chromosome

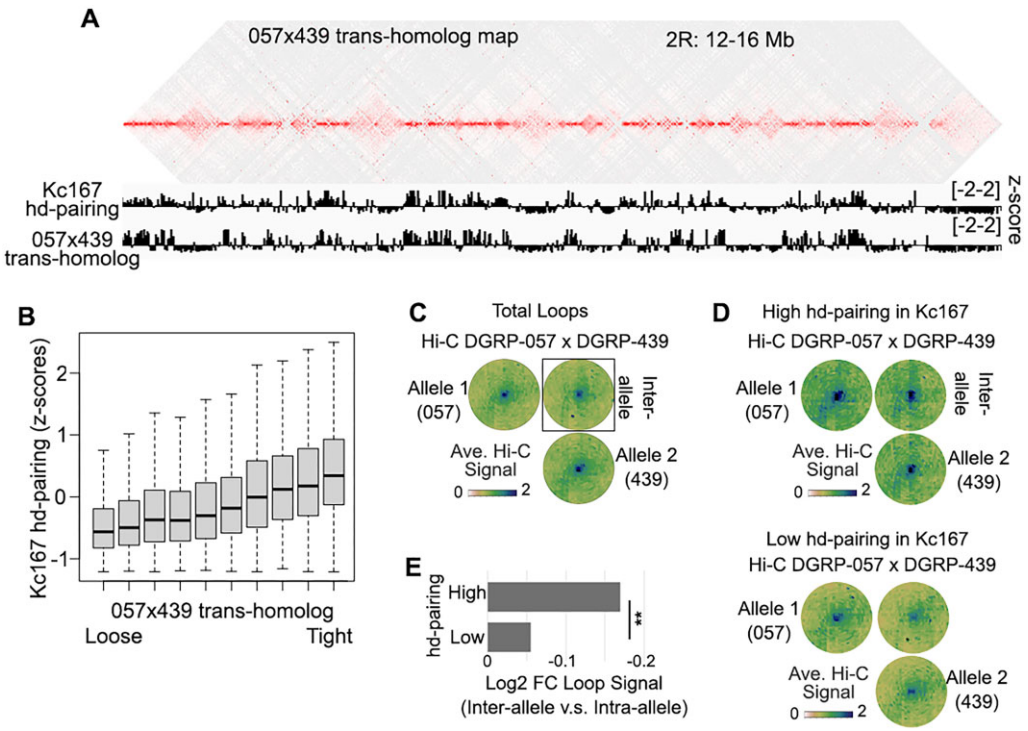

Figure 6. Pc-loop interactions in the DGRP-057 × 439 hybrid cell line are both intra-and inter-allelic. (**A**) View of the DGRP-057 × 439 trans-homolog map showing tight vs. loose pairing as reported in (12). The bottom tracks show the hd-pairing signal in Kc167 cells and the DGRP-057 × 439 trans-homolog contacts in 5 kb bins. Values were plotted as z-scores for comparison. (**B**) hd-pairing signal in Kc167 cells at *loci* categorized by deciles of trans-homolog contacts in the DGRP-057 × 439 hybrid cell line. (**C, D**) Average Hi-C signal in the DGRP-057 × 439 hybrid cell line is shown for the individual 057 and 439 alleles, as well as for the inter-allelic interactions. Signal is shown for the total Pc-loops (**C**), as well as for loops categorized as highly-paired or lowly-paired according to their hd-pairing signal in Kc167 cells (**D**). No significant difference was found comparing inter-allele to each intra-allele signal directly at anchors (center signals); $P > 0.05$ paired two-sample *t*-test for inter-allele versus allele 1 and inter-allele versus allele 2 in each panel. (**E**) Quantification of the $\log_2$ fold-ratio (FC) of inter-allele versus intra-allele signal shown in panel **D**. ** indicates $P \leq 0.01$ Monte Carlo permutation testing for the difference in high ($n = 39$) versus low ($n = 42$) hd-pairing Pc loops.

condensation since osmostress is known to increase chromatin condensation (31–33), while, like depletion of CAP-H2 (25,61), Z4 depletion partially reduces axial chromatin compaction. Thus, though counterintuitive, it is possible that chromatin condensation negatively regulates intra-chromosomal 3D interactions. However, in the case of Pc-loops, the observation that pairing correlates with loop-strength under normal physiological conditions argues against this possibility. Further work will help to clarify these questions.

Data availability

The accession numbers of the ChIP-seq, Hi-C, and ATAC-seq data generated in this work are GEO: GSE213553. Code can be obtained from https://zenodo.org/doi/10.5281/zenodo.10783405. Code can also be obtained from https://github.com/JRowleyLab/hdpairing. APBS ChIP-seq datasets were GSE30740; GSE63518; GSE54529; GSE80702 from (26,35,70,71). Pc ChIP-seq data set was GSE63518 from (35). MRG15 peaks in Kc167 cells were obtained from modENCODE (58) accession GSE25366 and converted to dm6 using liftOver (53). Haplotype resolved Hi-C for 057 × 439 hybrid cells was GSE121255 (12).

Supplementary data

Supplementary Data are available at NAR Online.

Acknowledgements

We thank Drs Ting Wu and Jumana AlHaj Abed for helpful discussions during the preparation of this manuscript. We also thank Dr Victor Corces for antibodies, training and helpful discussions, and Drs Anja C. Nagel, Asifa Akhtar and Lluisa Espinàs for antibodies. We also acknowledge the help of the IRB Functional Genomics and Advanced Digital Microscopy facilities.

Funding

MICIN/AEI 10.13039/501100011033 [PGC2018-094538-B-100 and PID2021-123303NB-I00], 'FEDER, una manera de hacer Europa' and the Generalitat de Catalunya [SGR2014-204 and SGR2017-475] to F.A.; Spanish Ministry of Economy and Competitiveness [PID2021-124723NB-C21 and PID2021-124723NB-C22], Unidad de Excelencia Maria de Maeztu [MDM-2014-0370] to UPF and ICREA Acadèmia (Catalan Government) to F.P. and E.N. European Union's Horizon 2020 Research and Innovation Programme under the Marie Skłodowska-Curie [754510] to S.T.; National Institutes of Health Pathway to Independence Award [R00GM1287671] and NIH Maximizing Investigators' Research Award [R35GM147467] to M.J.R.; M.P., P.B., J.P.-R. acknowledge receipt of FPI fellowships from MICIN/AEI [10.13039/501100011033] and 'FEDER, una manera de hacer Europa'. The content is solely the responsibility of the authors and does not necessarily represent the official views

of the NIH. Funding for open access charge: NIH [MIRA R35GM147467].

Conflict of interest statement

None declared.

References

1. Rowley,M.J. and Corces,V.G. (2018) Organizational principles of 3D genome architecture. *Nat. Rev. Genet.*, **19**, 789–800.
2. Abdennur,N. and Mirny,L.A. (2020) Cooler: scalable storage for Hi-C data and other genomically labeled arrays. *Bioinformatics*, **36**, 311–316.
3. Yatskevich,S., Rhodes,J. and Nasmyth,K. (2019) 0rganization of chromosomal DNA by SMC complexes. *Annu. Rev. Genet.*, **53**, 445–482.
4. Skibbens,R.V. (2008) Mechanisms of sister chromatid pairing. *Int. Rev. Cell Mol. Biol.*, **269**, 284–339.
5. McKee,B.D. (2004) Homologous pairing and chromosome dynamics in meiosis and mitosis. *Biochim. Biophys. Acta*, **1677**, 165–180.
6. Apte,M.S. and Meller,V.H. (2012) Homologue pairing in flies and mammals: gene regulation when two are involved. *Genet Res. Int.*, **2012**, 430587.
7. Joyce,E.F., Erceg,J. and Wu,C.T. (2016) Pairing and anti-pairing: a balancing act in the diploid genome. *Curr. Opin. Genet. Dev.*, **37**, 119–128.
8. Metz,C.W. (1916) Chromosome studies on the Diptera: II. The paired association of chromosomes in the Diptera and its significance. *J. Exp. Zool.*, **21**, 213–279.
9. Rosin,L.F., Nguyen,S.C. and Joyce,E.F. (2018) Condensin II drives large-scale folding and spatial partitioning of interphase chromosomes in Drosophila nuclei. *PLoS Genet.*, **14**, e1007393.
10. Hartl,T.A., Smith,H.F. and Bosco,G. (2008) Chromosome alignment and transvection are antagonized by condensin II. *Science*, **322**, 1384–1387.
11. Rowley,M.J., Lyu,X., Rana,V., Ando-Kuri,M., Karns,R., Bosco,G. and Corces,V.G. (2019) Condensin II counteracts cohesin and RNA polymerase II in the establishment of 3D chromatin organization. *Cell Rep.*, **26**, 2890–2903.
12. AlHaj Abed,J., Erceg,J., Goloborodko,A., Nguyen,S.C., McCole,R.B., Saylor,W., Fudenberg,G., Lajoie,B.R., Dekker,J., Mirny,L.A., *et al.* (2019) Highly structured homolog pairing reflects functional organization of the Drosophila genome. *Nat. Commun.*, **10**, 4485.
13. Child,M.B.t., Bateman,J.R., Jahangiri,A., Reimer,A., Lammers,N.C., Sabouni,N., Villamarin,D., McKenzie-Smith,G.C., Johnson,J.E., Jost,D., *et al.* (2021) Live imaging and biophysical modeling support a button-based mechanism of somatic homolog pairing in Drosophila. *eLife*, **10**, e64412.
14. Erceg,J., AlHaj Abed,J., Goloborodko,A., Lajoie,B.R., Fudenberg,G., Abdennur,N., Imakaev,M., McCole,R.B., Nguyen,S.C., Saylor,W., *et al.* (2019) The genome-wide multi-layered architecture of chromosome pairing in early Drosophila embryos. *Nat. Commun.*, **10**, 4486.
15. Fujioka,M., Mistry,H., Schedl,P. and Jaynes,J.B. (2016) Determinants of Chromosome Architecture: insulator Pairing in cis and in trans. *PLoS Genet.*, **12**, e1005889.
16. Peterson,S.C., Samuelson,K.B. and Hanlon,S.L. (2021) Multi-scale organization of the Drosophila melanogaster genome. *Genes (Basel)*, **12**, 817.
17. Viets,K., Sauria,M.E.G., Chernoff,C., Rodriguez Viales,R., Echterling,M., Anderson,C., Tran,S., Dove,A., Goyal,R., Voortman,L., *et al.* (2019) Characterization of button loci that promote homologous chromosome pairing and cell-type-specific interchromosomal gene regulation. *Dev. Cell*, **51**, 341–356.
18. Geyer,P.K., Green,M.M. and Corces,V.G. (1990) Tissue-specific transcriptional enhancers may act in trans on the gene located in the homologous chromosome: the molecular basis of transvection in Drosophila. *EMBO J.*, **9**, 2247–2256.
19. Lim,B., Heist,T., Levine,M. and Fukaya,T. (2018) Visualization of transvection in living Drosophila embryos. *Mol. Cell*, **70**, 287–296.
20. Williams,B.R., Bateman,J.R., Novikov,N.D. and Wu,C.T. (2007) Disruption of topoisomerase II perturbs pairing in Drosophila cell culture. *Genetics*, **177**, 31–46.
21. Joyce,E.F., Williams,B.R., Xie,T. and Wu,C.T. (2012) Identification of genes that promote or antagonize somatic homolog pairing using a high-throughput FISH-based screen. *PLoS Genet.*, **8**, e1002667.
22. Bosco,G. (2012) Chromosome pairing: a hidden treasure no more. *PLoS Genet.*, **8**, e1002737.
23. King,T.D., Leonard,C.J., Cooper,J.C., Nguyen,S., Joyce,E.F. and Phadnis,N. (2019) Recurrent losses and rapid evolution of the condensin II complex in insects. *Mol. Biol. Evol.*, **36**, 2195–2204.
24. Nguyen,H.Q., Nye,J., Buster,D.W., Klebba,J.E., Rogers,G.C. and Bosco,G. (2015) Drosophila casein kinase I alpha regulates homolog pairing and genome organization by modulating condensin II subunit Cap-H2 levels. *PLoS Genet.*, **11**, e1005014.
25. Smith,H.F., Roberts,M.A., Nguyen,H.Q., Peterson,M., Hartl,T.A., Wang,X.J., Klebba,J.E., Rogers,G.C. and Bosco,G. (2013) Maintenance of interphase chromosome compaction and homolog pairing in Drosophila is regulated by the condensin cap-h2 and its partner Mrg15. *Genetics*, **195**, 127–146.
26. Cubeñas-Potts,C., Rowley,M.J., Lyu,X., Li,G., Lei,E.P. and Corces,V.G. (2016) Different enhancer classes in Drosophila bind distinct architectural proteins and mediate unique chromatin interactions and 3D architecture. *Nucleic Acids Res.*, **45**, 1714–1730.
27. Rowley,M.J., Nichols,M.H., Lyu,X., Ando-Kuri,M., Rivera,I.S.M., Hermetz,K., Wang,P., Ruan,Y. and Corces,V.G. (2017) Evolutionarily conserved principles predict 3D chromatin organization. *Mol. Cell*, **67**, 837–852.
28. Gutierrez-Perez,I., Rowley,M.J., Lyu,X., Valadez-Graham,V., Vallejo,D.M., Ballesta-Illan,E., Lopez-Atalaya,J.P., Kremsky,I., Caparros,E., Corces,V.G., *et al.* (2019) Ecdysone-induced 3D chromatin reorganization involves active enhancers bound by Pipsqueak and Polycomb. *Cell Rep.*, **28**, 2715–2727.
29. Ogiyama,Y., Schuettengruber,B., Papadopoulos,G.L., Chang,J.M. and Cavalli,G. (2018) Polycomb-dependent chromatin looping contributes to gene silencing during Drosophila development. *Mol. Cell*, **71**, 73–88.
30. Eagen,K.P., Aiden,E.L. and Kornberg,R.D. (2017) Polycomb-mediated chromatin loops revealed by a subkilobase-resolution chromatin interaction map. *Proc. Natl. Acad. Sci. U.S.A.*, **114**, 8764–8769.
31. Schoborg,T., Rickels,R., Barrios,J. and Labrador,M. (2013) Chromatin insulator bodies are nuclear structures that form in response to osmotic stress and cell death. *J. Cell Biol.*, **202**, 261–276.
32. Belyi,A.A., Alekseev,A.A., Fedintsev,A.Y., Balybin,S.N., Proshkina,E.N., Shaposhnikov,M.V. and Moskalev,A.A. (2020) The resistance of Drosophila melanogaster to oxidative, genotoxic, proteotoxic, osmotic stress, infection, and starvation depends on age according to the stress factor. *Antioxidants (Basel)*, **9**, 1239.
33. Finan,J.D. and Guilak,F. (2010) The effects of osmotic stress on the structure and function of the cell nucleus. *J. Cell. Biochem.*, **109**, 460–467.
34. Amat,R., Bottcher,R., Le Dily,F., Vidal,E., Quilez,J., Cuartero,Y., Beato,M., de Nadal,E. and Posas,F. (2019) Rapid reversible changes in compartments and local chromatin organization revealed by hyperosmotic shock. *Genome Res.*, **29**, 18–28.
35. Li,L., Lyu,X., Hou,C., Takenaka,N., Nguyen,H.Q., Ong,C.T., Cubenas-Potts,C., Hu,M., Lei,E.P., Bosco,G., *et al.* (2015) Widespread rearrangement of 3D chromatin organization underlies polycomb-mediated stress-induced silencing. *Mol. Cell*, **58**, 216–231.
36. Kugler,S.J. and Nagel,A.C. (2007) Putzig is required for cell proliferation and regulates notch activity in Drosophila. *Mol. Biol. Cell*, **18**, 3733–3740.

37. Raja,S.J., Charapitsa,I., Conrad,T., Vaquerizas,J.M., Gebhardt,P., Holz,H., Kadlec,J., Fraterman,S., Luscombe,N.M. and Akhtar,A. (2010) The nonspecific lethal complex is a transcriptional regulator in Drosophila. *Mol. Cell*, **38**, 827–841.
38. Batlle,M., Marsellach,F.X., Huertas,D. and Azorin,F. (2011) Drosophila vigilin, DDP1, localises to the cytoplasm and associates to the rough endoplasmic reticulum. *Biochim. Biophys. Acta*, **1809**, 46–55.
39. Silva-Sousa,R., Lopez-Panades,E., Pineyro,D. and Casacuberta,E. (2012) The chromosomal proteins JIL-1 and Z4/Putzig regulate the telomeric chromatin in Drosophila melanogaster. *PLoS Genet.*, **8**, e1003153.
40. Moreno-Moreno,O., Torras-Llort,M. and Azorin,F. (2006) Proteolysis restricts localization of CID, the centromere-specific histone H3 variant of Drosophila, to centromeres. *Nucleic Acids Res.*, **34**, 6247–6255.
41. Kessler,R., Tisserand,J., Font-Burgada,J., Reina,O., Coch,L., Attolini,C.S., Garcia-Bassets,I. and Azorin,F. (2015) dDsk2 regulates H2Bub1 and RNA polymerase II pausing at dHP1c complex target genes. *Nat. Commun.*, **6**, 7049.
42. Wallace,H.A., Klebba,J.E., Kusch,T., Rogers,G.C. and Bosco,G. (2015) Condensin II regulates interphase chromatin organization through the Mrg-binding motif of Cap-H2. *G3*, **5**, 803–817.
43. Langmead,B. and Salzberg,S.L. (2012) Fast gapped-read alignment with Bowtie 2. *Nat. Methods*, **9**, 357–359.
44. Zhang,Y., Liu,T., Meyer,C.A., Eeckhoute,J., Johnson,D.S., Bernstein,B.E., Nussbaum,C., Myers,R.M., Brown,M., Li,W., *et al.* (2008) Model-based analysis of ChIP-Seq (MACS). *Genome Biol.*, **9**, R137.
45. Dickson,B.M., Tiedemann,R.L., Chomiak,A.A., Cornett,E.M., Vaughan,R.M. and Rothbart,S.B. (2020) A physical basis for quantitative ChIP-sequencing. *J. Biol. Chem.*, **295**, 15826–15837.
46. Zeitlinger,J., Stark,A., Kellis,M., Hong,J.W., Nechaev,S., Adelman,K., Levine,M. and Young,R.A. (2007) RNA polymerase stalling at developmental control genes in the Drosophila melanogaster embryo. *Nat. Genet.*, **39**, 1512–1516.
47. Ramirez,F., Dundar,F., Diehl,S., Gruning,B.A. and Manke,T. (2014) deepTools: a flexible platform for exploring deep-sequencing data. *Nucleic Acids Res.*, **42**, W187–W191.
48. Rao,S.S.P., Huntley,M.H., Durand,N.C., Stamenova,E.K., Bochkov,I.D., Robinson,J.T., Sanborn,A.L., Machol,I., Omer,A.D., Lander,E.S., *et al.* (2014) A 3D map of the human genome at kilobase resolution reveals principles of chromatin looping. *Cell*, **159**, 1665–1680.
49. Servant,N., Varoquaux,N., Lajoie,B.R., Viara,E., Chen,C.J., Vert,J.P., Heard,E., Dekker,J. and Barillot,E. (2015) HiC-Pro: an optimized and flexible pipeline for Hi-C data processing. *Genome Biol.*, **16**, 259.
50. Durand,N.C., Robinson,J.T., Shamim,M.S., Machol,I., Mesirov,J.P., Lander,E.S. and Aiden,E.L. (2016) Juicebox provides a visualization system for Hi-C contact maps with unlimited zoom. *Cell Syst.*, **3**, 99–101.
51. Wang,J. and Nakato,R. (2022) HiC1Dmetrics: framework to extract various one-dimensional features from chromosome structure data. *Brief Bioinform.*, **23**, bbab509.
52. Rowley,M.J., Poulet,A., Nichols,M.H., Bixler,B.J., Sanborn,A.L., Brouhard,E.A., Hermetz,K., Linsenbaum,H., Csankovszki,G., Lieberman Aiden,E., *et al.* (2020) Analysis of Hi-C data using SIP effectively identifies loops in organisms from C. elegans to mammals. *Genome Res.*, **30**, 447–458.
53. Raney,B.J., Barber,G.P., Benet-Pages,A., Casper,J., Clawson,H., Cline,M.S., Diekhans,M., Fischer,C., Navarro Gonzalez,J., Hickey,G., *et al.* (2023) The UCSC Genome Browser database: 2024 update. *Nucleic Acids Res.*, **52**, D1082-D1088.
54. Buenrostro,J.D., Wu,B., Chang,H.Y. and Greenleaf,W.J. (2015) ATAC-seq: a Method for Assaying Chromatin Accessibility Genome-Wide. *Curr. Protoc. Mol. Biol.*, **109**, 21.29.1–21.29.9.
55. Martin,M. (2011) Cutadapt removes adapter sequences from high-throughput sequencing reads. *EMBnet.journal*, **17**, 10–12.
56. Shao,Z., Zhang,Y., Yuan,G.C., Orkin,S.H. and Waxman,D.J. (2012) MAnorm: a robust model for quantitative comparison of ChIP-Seq data sets. *Genome Biol.*, **13**, R16.
57. Schep,A.N., Buenrostro,J.D., Denny,S.K., Schwartz,K., Sherlock,G. and Greenleaf,W.J. (2015) Structured nucleosome fingerprints enable high-resolution mapping of chromatin architecture within regulatory regions. *Genome Res.*, **25**, 1757–1770.
58. mod,E.C., Roy,S., Ernst,J., Kharchenko,P.V., Kheradpour,P., Negre,N., Eaton,M.L., Landolin,J.M., Bristow,C.A., Ma,L., *et al.* (2010) Identification of functional elements and regulatory circuits by Drosophila modENCODE. *Science*, **330**, 1787–1797.
59. Jung,Y.H., Kremsky,I., Gold,H.B., Rowley,M.J., Punyawai,K., Buonanotte,A., Lyu,X., Bixler,B.J., Chan,A.W.S. and Corces,V.G. (2019) Maintenance of CTCF- and transcription factor-mediated interactions from the gametes to the early mouse embryo. *Mol. Cell.*, **75**, 154–171.
60. Jung,Y.H., Sauria,M.E.G., Lyu,X., Cheema,M.S., Ausio,J., Taylor,J. and Corces,V.G. (2017) Chromatin states in mouse sperm correlate with embryonic and adult regulatory landscapes. *Cell Rep.*, **18**, 1366–1382.
61. Bauer,C.R., Hartl,T.A. and Bosco,G. (2012) Condensin II promotes the formation of chromosome territories by inducing axial compaction of polyploid interphase chromosomes. *PLoS Genet.*, **8**, e1002873.
62. George,C.M., Bozler,J., Nguyen,H.Q. and Bosco,G. (2014) Condensins are required for maintenance of nuclear architecture. *Cells*, **3**, 865–882.
63. Green,L.C., Kalitsis,P., Chang,T.M., Cipetic,M., Kim,J.H., Marshall,O., Turnbull,L., Whitchurch,C.B., Vagnarelli,P., Samejima,K., *et al.* (2012) Contrasting roles of condensin I and condensin II in mitotic chromosome formation. *J. Cell Sci.*, **125**, 1591–1604.
64. Lyu,X., Rowley,M.J. and Corces,V.G. (2018) Architectural proteins and pluripotency factors cooperate to orchestrate the transcriptional response of hESCs to temperature stress. *Mol. Cell*, **71**, 940–955.
65. Lieberman-Aiden,E., van Berkum,N.L., Williams,L., Imakaev,M., Ragoczy,T., Telling,A., Amit,I., Lajoie,B.R., Sabo,P.J., Dorschner,M.O., *et al.* (2009) Comprehensive mapping of long-range interactions reveals folding principles of the human genome. *Science*, **326**, 289–293.
66. Leidescher,S., Ribisel,J., Ullrich,S., Feodorova,Y., Hildebrand,E., Galitsyna,A., Bultmann,S., Link,S., Thanisch,K., Mulholland,C., *et al.* (2022) Spatial organization of transcribed eukaryotic genes. *Nat. Cell Biol.*, **24**, 327–339.
67. O'Sullivan,J.M., Tan-Wong,S.M., Morillon,A., Lee,B., Coles,J., Mellor,J. and Proudfoot,N.J. (2004) Gene loops juxtapose promoters and terminators in yeast. *Nat. Genet.*, **36**, 1014–1018.
68. Chowdhary,S., Kainth,A.S. and Gross,D.S. (2017) Heat shock protein genes undergo dynamic alteration in their three-dimensional structure and genome organization in response to thermal stress. *Mol. Cell. Biol.*, **37**, 24.
69. Hiraoka,Y. (2020) Phase separation drives pairing of homologous chromosomes. *Curr. Genet.*, **66**, 881–887.
70. Van Bortle,K., Nichols,M.H., Li,L., Ong,C.T., Takenaka,N., Qin,Z.S. and Corces,V.G. (2014) Insulator function and topological domain border strength scale with architectural protein occupancy. *Genome Biol.*, **15**, R82.
71. Yang,J., Sung,E., Donlin-Asp,P.G. and Corces,V.G. (2013) A subset of Drosophila Myc sites remain associated with mitotic chromosomes colocalized with insulator proteins. *Nat. Commun.*, **4**, 1464.

Received: October 24, 2023. **Revised:** February 16, 2024. **Editorial Decision:** March 4, 2024. **Accepted:** March 7, 2024